Indicator for Bearing Fault Detection in Asynchronous Motors using Stator Current Spectral Analysis

Baptiste Trajin, *IEEE Student Member*
Université de Toulouse;
LAPLACE; CNRS, INPT, UPS;
2 rue Charles Camichel BP7122
31071 Toulouse Cedex 07, France
Email: baptiste.trajin@laplace.univ-tlse.fr

Jeremi Regnier, *IEEE Member*
Université de Toulouse;
LAPLACE; CNRS, INPT, UPS;
2 rue Charles Camichel BP7122
31071 Toulouse Cedex 07, France
Email: jeremi.regnier@laplace.univ-tlse.fr

Jean Faucher, *IEEE Member*
Université de Toulouse;
LAPLACE; CNRS, INPT, UPS;
2 rue Charles Camichel BP7122
31071 Toulouse Cedex 07, France
Email: jean.faucher@laplace.univ-tlse.fr

***Abstract*— This paper deals with the application of motor current spectral analysis for the detection of artificially damaged rolling bearings in asynchronous machine. Vibration monitoring of mechanical characteristic frequencies related to the bearings is widely used to detect faulty operations. However, vibration measurement is expensive and can not always be performed. An alternative is to base the monitoring on the available electrical quantities e.g. the machine stator current which is often already measured for control and protection purposes. The bearing faults reveal the presence of mechanical load torque oscillations. A theoretical stator current model in case of load torque oscillations demonstrates the presence of phase modulation. Related sideband components appear in the current spectrum and can be used for detection. Experimental measurements show that their amplitudes are linked to the fault frequency by a transfer function including resonance. This singularity will be used to improve the detection efficiency. Fault detectors using the energy of stator current in specific frequency ranges are then proposed. The efficiency of indicators is studied on long and short data records of experimental current for different bearing faults. The most significant of the investigated indicators is finally improved to guarantee a higher reliability of the detection.**

I. Introduction

Electrical drives using induction motors are widely used in many industrial applications because of their low cost and high robustness. However, faulty operations could be induced by bearing faults [1, 2]. To improve the availability and reliability of the drive, a condition monitoring could be implemented to favor the predictive maintenance. Traditionally, motor condition is supervised using vibration analysis but measuring such mechanical quantities to detect bearing faults is often expensive. To overcome this problem, available electrical quantities such as stator current could be used. A general review of monitoring and fault diagnosis schemes using stator current can be found in [3]. Concerning bearings fault detection, several studies demonstrate that specific signatures appear on stator current spectrum [4, 5]. However, few papers concern the definition of an indicator performing an automatic extraction of relevant information from the current spectrum. The present work deals with these specific aspects.

Natural bearing faults can be due for example to corrosion, contamination, ineffective lubrification or electric arcing induced by the use of PWM voltage source [6, 7]. Then, artificially damaged bearings are made to be realistic regarding to such critical faults. A model for bearing fault detection has been proposed in [8] based on the assumption that bearing defects lead to variations of the physical air gap. Other studies consider that bearing faults induce load torque oscillations [9].

In this paper, the load torque oscillation approach is used. Section II presents a short overview of bearing faults. Measurements of torque are then performed to point out that load torque oscillations appear at characteristic frequencies under faulty conditions. A stator current model, using the magnetomotive force approach, is used to demonstrate that sideband components due to load torque oscillations exist in the current spectrum. An experimental Bode diagram useful for detection purposes is proposed to study the amplitude of these specific sidebands related to torque oscillation frequencies. In section III, the issue of the definition of automatic detectors based on current spectral energy estimation is recalled [10]. Using experimental results with artificially damaged bearings, several basic indicators are proposed on long data records for off-line monitoring and their efficiencies are compared. In order to be more realistic with regard to a real time implantation, the section IV deals with the exploitation of the proposed indicators on short data record. Experimental results show that shorter data induce a lower reliability of the detectors. The section V proposes techniques to improve the detector efficiency of the best indicator identified in section IV by reducing its standard deviation. Once again, experimental results demonstrate the ability of the proposed detection scheme to distinguish healthy and faulty bearings.

II. Load torque oscillations

A. Bearing faults frequencies

As a matter of fact, frequencies that could appear in vibration spectrum with appearance of bearing's faults are theoretically well known. Only the low frequency ranges

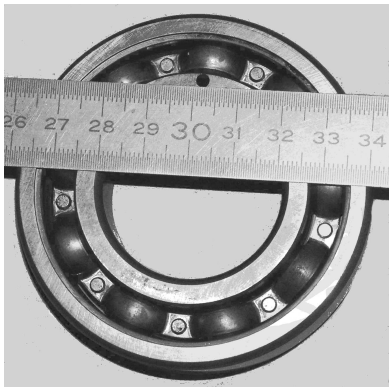

Fig. 1. Photograph of the faulty bearing with localized inner race fault

($< 1kHz$) rendering defects which are related to the rotating speed like bearing faults are considered. The next point is that harmonics due to defects could appear as combinations of mechanical rotating frequency and characteristic frequencies expressed by (1) [2, 11].

$$\begin{aligned} f_{orf} &= \frac{f_r}{2} N_b \Big(1 - \frac{D_b \cos\theta}{D_p}\Big) \\ f_{irf} &= \frac{f_r}{2} N_b \Big(1 + \frac{D_b \cos\theta}{D_p}\Big) \\ f_c &= \frac{f_r}{2} \Big(1 - \frac{D_b \cos\theta}{D_p}\Big) \end{aligned} \tag{1}$$

where:

- f_{orf} outer race fault frequency;
- f_{irf} inner race fault frequency;
- f_c cage frequency;
- f_r mechanical rotating frequency;
- N_b number of balls;
- D_b ball diameter;
- D_p pitch diameter;
- θ contact angle.

B. Load torque oscillations due to bearing faults

6208-type bearings are modified using electro-erosion to create a localized outer or inner race defect. Then, the fault consists in a $3mm$-large hole in the full width of the outer or inner raceway (see Fig. 1). The single point defect can be considered as the worst case of bearing wear due to ineffective lubrification [7]. The experimental setup is composed of a $5.5kW$ induction machine supplied by a variable frequency inverter. Faulty bearings are mounted in the machine under test and an acquisition board is used to sample the torque and the stator currents.

First of all, the effects of bearing faults on mechanical load torque are required. Experimental spectrum of load torque demonstrates the presence of harmonics at frequencies related to bearing faults. Here, the mechanical speed is chosen equal to the nominal one namely $25Hz$. The outer race fault frequency equals $89Hz$ and the inner race frequency equals $136Hz$. Hence, Figs. 2(a) and 2(b) show a part of the mechanical torque spectrum around twice the characteristic fault frequency for outer and inner race fault respectively compared to the healthy case.

C. Stator current model

Previous studies on mechanical failures in induction motors have shown that load torque oscillations induce phase modulations (PM) on stator current [9, 12, 13]. Considering that the load torque oscillation is composed of a single harmonic at the pulsation ω_{osc}, the load torque on the shaft of the machine can be expressed using (2) as an average torque equal to the electromagnetic motor torque and a sinusoidal component of amplitude Γ_c :

$$\Gamma_{load}(t) = \Gamma_0 + \Gamma_c \cos(\omega_{osc} t) \tag{2}$$

Physically, the mechanical equation linking torque to mechanical angular position proves that load torque oscillations cause angular position oscillations. Here, the mechanical transfer function is equal to a simple inertia without friction or stiffness term plus an integrator. The mechanical position is used to calculate the rotor magnetomotive forces (MMF). Thus, the magnetic field in the airgap is obtained by the product between the airgap permeance Λ_0, considered as a constant (along time and position), and the rotor and stator MMF. The magnetic field is integrated on the coil's surface of a stator winding in order to determine the airgap flux density in the coil. Hence, variation of flux with time in a stator winding leads to induced voltage. The stator current expression (3) for an arbitrary phase ϕ_s is then obtained considering a linear relation between current and induced voltage. In (3), ω_s is the stator current fundamental pulsation, I_s the amplitude of stator current, I_r the amplitude of rotor current, p the number of pole pairs of the asynchronous machine and J the inertia.

$$i(t) = I_s \cos(\omega_s t + \phi_s) + I_r \sin\Big(\omega_s t + p\frac{\Gamma_c}{J\omega_{osc}^2}\cos(\omega_{osc} t)\Big) \tag{3}$$

In (3), the first term is related to the stator MMF contribution and the second one, including the phase modulation of stator current, is related to the rotor MMF contribution. If the amplitude of the torque oscillation is pretty small, the Fourier Transform (FT) of the stator current can be expressed using (4) along the frequency ν.

$$FT\{i(t)\} = (I_s + I_r)\delta(\nu - f_s) + I_r p\frac{\Gamma_c}{2J\omega_{osc}^2}\delta\Big(\nu - (f_s \pm f_{osc})\Big) \tag{4}$$

Moreover, notice that in case of faulty bearings, the frequency of load torque oscillations f_{osc} can equal any of combinations of characteristic fault frequencies underlined by the load torque spectrum.

D. Amplitude variation law of sideband components

The knowledge of the variation law between stator current sideband amplitude and fault frequency is important for detection purpose. The link between PM harmonics amplitudes of the stator current (i.e. stator current sideband modulation energy) and load torque oscillation frequencies is then studied.

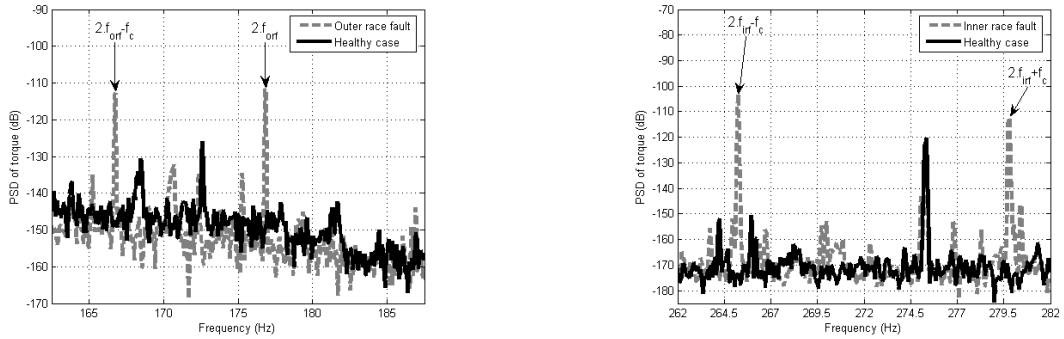

(a) (b)

Fig. 2. Spectrum of mechanical torque - Comparison between healthy and faulty cases

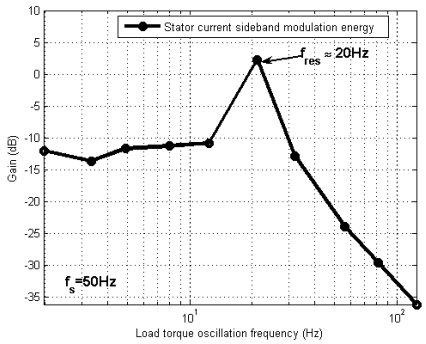

Fig. 3. Gain Bode diagram of experimental transfer function between load torque oscillations frequency and sideband components on stator currents

In order to draw a Bode diagram, the asynchronous motor is coupled to a DC motor. The DC machine is connected to a resistor through a DC/DC converter which controls the DC motor armature current. Hence, the DC motor produces load torque oscillations if the current reference of the control loop is composed of a DC offset plus an oscillation. The supply frequency of the asynchronous motor is constant and equals the nominal one $f_s = 50Hz$. Mechanical torque is measured with a torque sensor to check the induced load torque oscillation amplitude and frequency. Sideband component amplitudes of stator current are measured by off-line spectral analysis. The experimental gain Bode diagram shown in Fig. 3 is obtained by varying frequency of load torque oscillations. The main observation lies in the existence of a resonance point around $f_{res} = 20Hz$.

Single-point defects in ball bearings are related to characteristic frequencies determined in (1). Assuming that a single-point defect creates slight load torque oscillations at these frequencies, the resonance point is used as a natural amplifier to obtain higher PM harmonics on stator current. In order to use the resonance point, the supply frequency of the asynchronous machine is tuned to ensure that the theoretical mechanical fault frequency related to the localized fault of the bearing under test equals the resonance frequency noticed on the Bode diagram. In fact, with this approach, the PM modulation index shown in (4) will be amplified because of the electromechanical resonance. As a consequence, the fault detection efficiency on stator current will increase.

III. Definition of detectors for bearing faults

A. Definition of detectors I_1 and I_2

The fault detectors I_1 and I_2 are defined by extracting energies on frequency ranges corresponding to the sideband components at $f_s \pm f_{def}$ where f_{def} is either the inner or the outer theoretical mechanical fault frequency. Moreover, the frequency ranges are extended to include modulations linked to the mechanical speed and cage frequencies underlined by the mechanical load torque spectral analysis (see Fig. 2). The chosen frequency ranges are given in (5). The proposed indicator uses the relative error of energy between the current spectrum in faulty and healthy case in the specified frequency ranges.

$$\begin{array}{c} |f_s \pm [nf_{def} - \Delta f_c; nf_{def} + \Delta f_c]| \\ |f_s \pm [nf_{def} - f_r - \Delta f_c; nf_{def} - f_r + \Delta f_c]| \\ |f_s \pm [nf_{def} + f_r - \Delta f_c; nf_{def} + f_r + \Delta f_c]| \end{array} \quad (5)$$

where $n \in [1; 5]$.

Two detectors are then investigated using $\Delta f = f_c$ and $\Delta f = f_c/2$ for I_1 and I_2 respectively.

According to ranges specified in (5) and the value of n, the energy is estimated in 15 frequency ranges for each of the considered characteristic fault frequencies (f_{orf} and f_{irf}). Then, as expressed in (6), the relative errors of energy extracted from outer and inner race fault frequencies ranges (ΔE_{orf} and ΔE_{irf} respectively) are added in order to obtain a single energy difference ΔE_{tot}.

$$\Delta E_{tot}(k) = \Delta E_{orf}(k) + \Delta E_{irf}(k),\ k \in [1; 15] \quad (6)$$

Finally, a cumulative sum of $\Delta E_{tot}(k)$ is used to build the indicator. Only the last value of the cumulative sum is considered as the detector value. As a consequence, the final detector value could not perform a distinction between inner and outer race fault but only provide a distinction between healthy and faulty case. The detection of inner or outer race

fault will only be done with the supply frequency which is tuned to equal the resonance frequency and one of the characteristic fault frequencies (f_{orf} or f_{irf}).

B. Definition of detector I_3

To reduce the complexity of the calculation of the detectors I_1 and I_2, another detector I_3 is also investigated. It only uses the energies in ranges around the characteristic fault frequencies modulations given by (7). The relative error of energy is estimated in 5 frequency ranges for each of the considered characteristic fault frequencies. Then the detector is built as previously described.

$$|f_s \pm [nf_{def} - f_c; nf_{def} + f_c]| \text{ where } n \in [1; 5] \quad (7)$$

C. Exploitation of the resonance point

To illustrate the calculation of the detector values, a detailed example is given for detector I_1 in case of an outer and inner race fault. The acquisition of the stator current is done during $80s$ using a sampling frequency of $6400Hz$. Three experimental conditions are tested, corresponding to three different supply frequencies. In Fig. 4(a), the supply frequency f_s is tuned to $13.3Hz$ in order to ensure $f_{orf} = f_{res}$. In Fig. 4(b), the supply frequency f_s is tuned to $6.7Hz$ to ensure $f_{irf} = f_{res}$. Finally, in Fig. 4(c) the supply frequency f_s is tuned to $50Hz$, corresponding to the nominal supply frequency. Each case uses a reference of energy obtained with a healthy bearing. The figures show cumulative sum corresponding to the computation of detector I_1.

From Figs. 4(a) and 4(b), the representation of the cumulative sum allows differentiating faulty conditions from healthy case. As expected, properly tuning the frequency supply leads to focus on inner or outer race fault. When f_s is set to guarantee $f_{orf} = f_{res}$, the detection of the outer race fault is ensured and reciprocally the detection of the inner race fault is ensured when f_s is set to guarantee $f_{irf} = f_{res}$. Moreover, the two figures underline that if the characteristic fault frequency does not equal the resonance frequency, the associated fault is not detected. Furthermore, the Fig. 4(c) underlines that distinction between healthy and faulty cases is not possible with this detector when the sideband components are strongly attenuated, according to the electromechanical transfer function depicted in Fig. 3.

IV. Study of detectors on short data length

To avoid an excessive time computation, the previous indicators are tested on stator current signals with limited length. To properly extract energies required for the indicator calculations, an adapted minimal frequency range of the current spectrum (from 0 to f_{max}) must be covered. The frequency f_{max}, related to the supply frequency f_s, is variable and can be evaluated thanks to the knowledge of the frequency ranges used by the indicators. The sampling frequency f_e is then chosen such as $f_e = 3f_{max}$. The length of the data records is defined to ensure a frequency resolution for the current spectrum lower than $0.1Hz$.

TABLE I
Mean and standard deviation of detectors $f_{orf} = f_{res}$

	Healthy case detectors (Mean; Standard deviation)	**Outer race fault detectors (Mean; Standard deviation)**
I_1	(-8.09; 154.63)	(143.68; 200.03)
I_2	(-6.64; 159.74)	(52.84; 189.63)
I_3	(-2.18; 109.66)	(92.24; 106.01)

The reference used in the indicators computation is obtained with a healthy bearing. Energies of the sidebands are extracted from ten signal spectrum and the mean of these values in each frequency range is chosen as a reference.

The previously defined indicators are applied to three different bearings. The first one is a healthy bearing, the second one is a faulty bearing with a single-point defect on outer race and the third one is a faulty bearing with a single-point defect on inner race.

A. Detection of outer race defect

First of all, the three indicators are studied for the detection of an outer race defect. The supply frequency of the asynchronous machine is set to equal the mechanical characteristic frequency of the outer race defect and the resonance frequency ($f_s = 13.3Hz$). Thus, the maximum frequency required to calculate the detectors is $f_{max} = 141.5Hz$. The sampling frequency is then $f_e = 3f_{max} = 424Hz$. The length of the data record is set to 8192 samples to ensure a frequency resolution lower than $0.1Hz$. The reference is built as previously mentioned. The indicator I_1 is computed along 70 records for healthy and outer race fault conditions. Means and standard deviation of the three detectors are given in Table I.

The mean values of the detectors for the healthy case are close to zero as expected. In case of outer race fault, the mean values of the detectors for 70 records allow to clearly distinguish healthy and faulty cases. The best sensitivity is noticed for the indicator I_1. All the indicators standard deviation values are high, leading to a low reproducibility and reliability of results.

B. Detection of inner race defect

The three indicators are now used for the detection of an inner race fault. The supply frequency of the asynchronous machine is set to equal the characteristic frequency of the inner race defect and the resonance frequency ($f_s = 6.7Hz$). Thus, the maximum frequency required to calculate the detectors is $f_{max} = 102.5Hz$. The sampling frequency is then $f_e = 3f_{max} = 307.5Hz$. The length of the data record is set to 4096 samples to ensure a frequency resolution lower than $0.1Hz$. A new reference is built for this operating point with a healthy bearing. Means and standard deviation of detectors for the healthy and the inner race fault cases are given in Table II.

The same conclusions as before can be done, except on the mean of I_1 in case of healthy bearing detection which is not

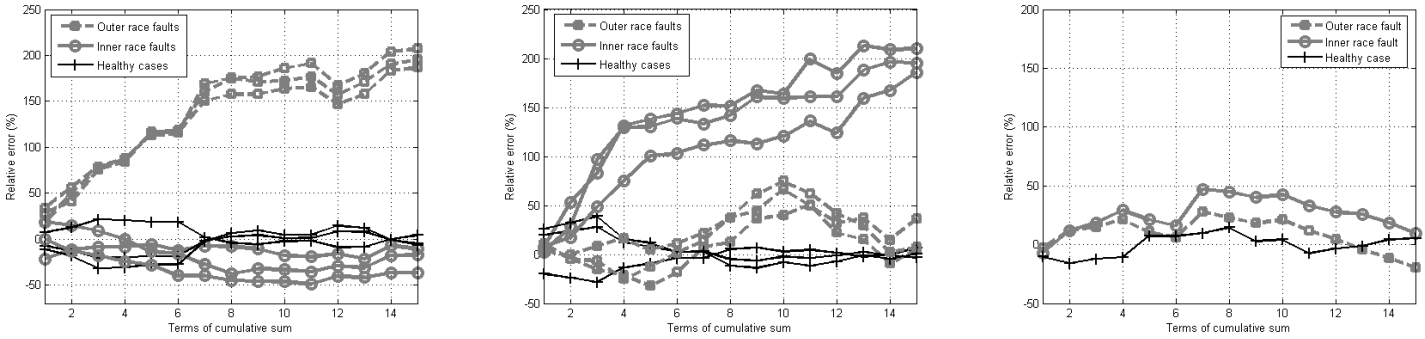

(a) $f_{orf} = f_{res}$ (b) $f_{irf} = f_{res}$ (c) $f_s = 50Hz$

Fig. 4. Cumulative sums of relative error in %

TABLE II
MEAN AND STANDARD DEVIATION OF DETECTORS WITH $f_{irf} = f_{res}$

	Healthy case detectors (Mean; Standard deviation)	**Inner race fault detectors (Mean; Standard deviation)**
I_1	(22.44; 137.76)	(98.41; 150.2)
I_2	(6.46; 184.78)	(22.64; 123.77)
I_3	(-1.96; 83.37)	(-0.14; 74.55)

close to zero. It underlines the fact that choosing a reference could significantly modify the values of the detectors.

Moreover, distinguish the inner fault becomes impossible with I_3. It means that fault frequencies in case of inner race fault often appear in combination with the mechanical rotating frequency.

Furthermore, even if the detection of bearing faults with I_2 seems to be possible, it could be noted that differences between faulty and healthy cases are lower than with I_1. This point is understandable because some fault harmonics which contain modulation at the cage frequency are neglected.

V. REDUCTION OF STANDARD DEVIATION OF THE DETECTOR

A. Choice of a detector

According to the previous results, the detector having the best sensitivity, whatever the considered bearing fault, is I_1. To reduce the standard deviation of this indicator, a sliding cumulative sum is performed. Each term of this sum is computed using a mean value of corresponding terms in the last N cumulative sums obtained while evaluating the last N indicator values. When a new data record is available, the sliding cumulative sum is computed again using the new cumulative sum obtained and the $N-1$ last cumulative sum. This principle is formulated using (8).

$$SUM_{K,j} = \frac{1}{N} \sum_{i=K}^{K+N-1} sum_{i,j} \tag{8}$$

where:

- $j \in [1; 15]$ represents the index of the terms of the cumulative sums;
- K is the index of the cumulative sum resulting from the meaning,
- N is the number of cumulative sums used for the meaning.

This method allows to reduce the standard deviation if the last term of the sliding cumulative sum is considered as the detector value. Obviously, the standard deviation significantly decreases when N increases. Applying a mean on $N = 40$ cumulative sums leads to a compromise between a low standard deviation and a high computational complexity. Therefore, experimental results for several of the faulty cases investigated show that this method could not be efficient enough. A final detector is built by calculating the mean of terms of the sliding cumulative sums as expressed in (9).

$$D_K = \frac{1}{N_B} \sum_{j=1}^{N_B} SUM_{K,j} \tag{9}$$

where N_B is the number of terms of the sliding cumulative sum.

This method permits to reduce significantly the standard deviation of detectors by reducing the weight of the last terms of the sliding cumulative sums which are related to high frequency phase modulations. Indeed, high frequency current modulations could be buried in noise because of the filtering effect of the transfer function shown on Fig. 3.

B. Detection of bearing faults

Figs. 5(a) and 5(b) show the histograms of 31 values of the detector D_K in outer and inner race fault respectively and healthy case for comparison. For each configuration, remember that a proper supply frequency is chosen to ensure the detection of one of the bearing fault type. Table III and IV give means and standard deviations of the detectors in case of outer and inner race fault detection respectively to verify that the detector efficiency is really improved. Standard deviation is strongly reduced. The healthy and faulty cases can be clearly distinguished with a good confidence rate.

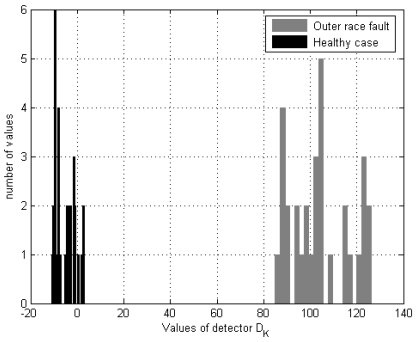

(a) $f_{orf} = f_{res}$

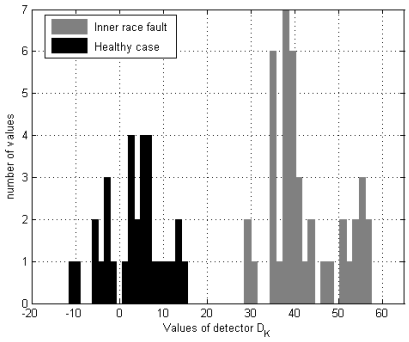

(b) $f_{irf} = f_{res}$

Fig. 5. Histogram of 31 values of detector D_K for healthy, outer and inner race fault cases

TABLE III
MEAN AND STANDARD DEVIATION OF D_K WITH $f_{orf} = f_{res}$

	Healthy case detectors (Mean; Standard deviation)	**Outer race fault detectors (Mean; Standard deviation)**
D_K	(-5.17; 4.27)	(104.01; 12.66)

TABLE IV
MEAN AND STANDARD DEVIATION OF D_K WITH $f_{irf} = f_{res}$

	Healthy case detector (Mean; Standard deviation)	**Inner race fault detector (Mean; Standard deviation)**
D_K	(3.35; 6.73)	(44.37; 7.58)

VI. CONCLUSION

In this paper, a novel method for an automatic detection of bearing faults in induction motors using stator current monitoring has been presented. As inner and outer race characteristic fault frequencies are well known, bearings are artificially damaged to ensure the assumption of localized faults. Using experimental results, measurements have shown that bearing defects induced load torque oscillations. Thus, a simplified model of stator current demonstrates that load torque oscillations lead to sideband components on stator current spectrum. The amplitude variation law of these signatures with respect to fault frequency, including a resonance, has been determined by experimental measurements. The resonance point has been used to allow to detect preferentially inner or outer race fault.

Three indicators have been proposed to extract the stator current spectral energy in frequency ranges related to bearing faults. According to computation complexity considerations, studies of the best indicator investigated have been conducted on short data length records. These studies have emphasized a low reproducibility and reliability of results. Consequently, some techniques have been introduced to reduce the standard deviations of the detectors. Finally, an automatic detector which allows to clearly distinguish healthy and faulty cases with a good confidence rate has been introduced and validated. To demonstrate the efficiency of the detector, more realistically damaged bearings will be studied in further work.

REFERENCES

[1] B. Raison, G. Rostaing, O. Butscher and C. -S. Maroni, *Investigations of algorithms for bearing fault detection in induction drives*, IEEE 28th Annual Conference of the Industrial Electronics Society, vol. 2, Nov. 2002, pp. 1696-1701.

[2] J. R. Stack, T. G. Habetler and R. G. Harley, *Fault classification and fault signature production for rolling element bearings in electric machines*, IEEE Transactions on Industry Applications, vol. 40, no. 3, May-Jun. 2004, pp. 735-739.

[3] S. Nandi and H. A. Toliyat, *Condition monitoring and fault diagnosis of electrical machines - a review*, IEEE Transactions on Energy Conversion, vol. 20, no. 4, Dec. 2005, pp. 719-729.

[4] J. R. Stack, R. G. Harley and T. G. Habetler, *An amplitude modulation detector for fault diagnosis in rolling element bearings*, IEEE Transactions on Industry Electronics, vol. 51, no. 5, Oct. 2004, pp. 1097-1102.

[5] R. R. Obaid, T. G. Habetler and J. R. Stack, *Stator current analysis for bearing damage detection in induction motors*, Symposium on Diagnostics for Electric Machines, Power Electronics and Drives, Aug. 2003, pp. 182-187.

[6] D. F. Busse, J. M. Erdman, R. J. Kerkman, D. W. Schlegel and G. L. Skibinski, *The effects of PWM voltage source inverters on the mechanical performance of rolling bearings*, IEEE Transactions on Industry Applications, vol. 33, no. 2, Mar-Apr. 1997, pp. 567-576.

[7] R. A. Guyer. "Rolling Bearings Handbook and Troubleshooting Guide", *Chilton Book Compagny*, Radnor, Pennsylvania, (1996).

[8] R. R. Schoen, T. G. Habetler, F. Kamran and R. G. Bartheld, *Motor bearing damage detection using stator current monitoring*, IEEE Transactions on Industry Applications, vol. 31, no. 6, Nov-Dec. 1995, pp. 1274-1279.

[9] M. Blodt, P. Granjon, B. Raison and G. Rostaing, *Models for bearing damage detection in induction motors using stator current monitoring*, IEEE International Symposium on Industrial Electronics, vol. 1, May 2004, pp. 383-388.

[10] B. Trajin, J. Regnier, J. Faucher, *Bearing Fault Indicator in Induction Machine Using Stator Current Spectral Analysis*, Power Electronics Machine and Dirves Conference, Apr. 2008, pp. 592-596.

[11] T. A. Harris, *Rolling bearing analysis*, Wiley, New-York, 3rd ed., 1991.

[12] R. R. Schoen and T. G. Habetler, *Effects of time-varying loads on rotor fault detection in induction machines*, IEEE Transactions on Industry Applications, vol. 31, no. 4, Jul-Aug. 1995, pp. 900-906.

[13] M. Blodt, J. Faucher, B. Dagues and M. Chabert, *Mechanical load fault detection in induction motors by stator current time-frequency analysis*, IEEE International Conference on Electric Machines and Drives, May 2005, pp. 1881-1888.